

The High-Temperature Oxidation Behavior of ODS-Fe₃Al

I. G. Wright*, B. A. Pint*, and P. F. Tortorelli*

ABSTRACT

The high-temperature oxidation behavior of an oxide dispersion-strengthened (ODS) Fe₃Al alloy has been studied during isothermal and cyclic exposures in oxygen and air over the temperature range 1000 to 1300°C. Compared to commercially-available ODS-FeCrAl alloys, it exhibited very similar short-term rates of oxidation at 1000 and 1100°C, but at higher temperatures the oxidation rate increased due to increased scale spallation. Over this temperature range the oxide scale formed was γ -Al₂O₃ with the morphological features typical of reactive element doping and was similar to those formed on the ODS-FeCrAl alloys. Although initially this scale appeared to be extremely adherent to the Fe₃Al substrate, an undulating metal-oxide interface formed with increasing time and temperature which led to cracking of the scale in the vicinity of surface undulations accompanied by a loss of small fragments of the full scale thickness. In some instances, the surface undulations appeared to have resulted from gross outward local extrusion of the alloy substrate. Similar features developed on the FeCrAl alloys, but they were typically much smaller after a given oxidation exposure. The oxide dispersion-strengthened Fe₃Al alloy has a significantly larger coefficient of thermal expansion (CTE) than typical FeCrAl alloys (approximately 1.5 times at 900°C), and this appears to be the major reason for the greater tendency for scale spallation. The stress generated by the CTE mismatch was apparently sufficient to lead to buckling and limited loss of scale at temperatures up to 1100°C, with an increasing amount of substrate deformation at 1200°C and above. This deformation led to increased scale spallation by producing an out-of-plane stress distribution, resulting in cracking or shearing of the oxide.

KEY WORDS: high-temperature oxidation; ODS-Fe₃Al; scale spallation

INTRODUCTION

Alloys based on Fe₃Al have long been of interest because of their good resistance to high-temperature oxidation and sulfidation, low density (Fe₃Al: 6.5 g/cm³), low materials cost and low content of strategic elements, as well as other properties such as high magnetic permeability and high electrical resistivity [see, for instance, ref. 1]. Good oxidation resistance results from the fact that the aluminum level of Fe₃Al-based alloys is significantly in excess of that required to ensure the formation of an essentially exclusively alumina scale under most conditions of exposure above about 500°C⁽²⁻⁶⁾. The predominant surface product that forms on iron aluminides between 600 and 800°C is reportedly γ -Al₂O₃⁽⁷⁾, but other forms such as α -Al₂O₃ may exist in this temperature range⁽⁸⁾. Transition to the slower growing α -Al₂O₃ occurs at approximately 900°C^(5,9).

A characteristic feature of the oxidation behavior of Fe₃Al is a tendency for scale spallation; DeVan⁽¹⁰⁾, for instance, reported that spallation resulted in the loss of a fine dust of oxide on cooling from reaction temperature. However, small additions of reactive elements (RE) such as Zr or Y made to Fe₃Al containing 2-5 at.% Cr have been found to promote very good long-term oxidation performance that approximately matches that of FeCrAlY alloys (and of RE-doped NiAl) at 1000 and 1100°C^(11,12). Without these oxygen-active elements, the scale spallation is significantly greater. When the RE is added as an oxide dispersion in powder metallurgically-produced alloys, Y₂O₃ appears to be most effective dispersoid in improving the oxide spallation behavior of Fe-28Al-2Cr (in atom percent)⁽¹¹⁾.

An oxide dispersion-strengthened (ODS) version of Fe₃Al (essentially Fe-28Cr-2Cr-0.5Y₂O₃) has been developed⁽¹³⁾ with the aim of achieving good high-temperature oxidation behavior and improved high-temperature creep strength. If this alloy has levels of high-temperature strength and creep resistance similar to commercial ODS-FeCrAl alloys (which will be the chief competitors for ODS-Fe₃Al in high-temperature, high creep-strength applications), it should also have the potential advantage of a longer oxidation-governed service life due to its inherently larger reservoir of

aluminum. This advantage will only be realized, however, if the rate of Al consumption from ODS-Fe₃Al to form the protective oxide scale is similar to that in the ODS -FeCrAl alloys.

In order to justify the expected high cost of ODS alloys, they must exhibit very long lifetimes at high temperatures. Few long-term oxidation data are available for any of these alloys^(14,15), and the established understanding of the oxidation behavior is based largely on relatively short-term studies. The results presented in this paper are taken from a study aimed at extending the characterization of the scale growth and morphology development of these alloys to longer times to provide a basis for understanding the modes of eventual breakdown and failure. Since this is a work in progress, it was considered useful to include some of the data generated for the competing ODS-FeCrAl alloys. A more extensive reporting of the results for the ODS-FeCrAl alloys is published elsewhere⁽¹⁶⁾.

EXPERIMENTAL PROCEDURES

ODS-Fe₃Al alloys were produced by ball-milling^(17,18) of pre-alloyed Fe₃Al powders with Y₂O₃ powder on a semi-production scale by Metallwerk Plansee (alloys designated PMWY-x). The alloys were consolidated by extrusion at 1000°C in mild steel cans at a reduction ratio of 9:1 to form 1.25 cm diameter rods. Alloys PMWY-1 and -2 were found to recrystallize upon annealing at 1200°C (> 4 h) or 1300°C (1 h) to develop the elongated grain structure required for high-temperature creep strength. Alloy PMWY-3 did not recrystallize even after >8 h at 1300°C⁽¹⁹⁾. Figure 1 shows the typical microstructure of these alloys in both the as-extruded (Fig. 1a) and recrystallized (Fig. 1b) conditions. Oxidation data are presented for alloys in both the as-extruded (fine-grained) and recrystallized (large-grained) conditions.

The chemical compositions of the ODS-Fe₃Al alloys studied, together with those for Kanthal APM and commercially available ODS-FeCrAl alloys, are listed in Table I. Kanthal APM was supplied in the form of 0.12 cm thick plate. This alloy is produced by a powder metallurgy technique that does not involve high-energy milling and is not considered an ODS alloy, although it has a composition similar to the commercial ODS-FeCrAl alloys. Chemical analysis indicated that it also contained a small addition of ZrO₂. Because of its consistently excellent oxidation behavior, it was included as a standard for comparison in this study. Inconel® Alloy MA956 was supplied by INCO Alloys Inc. in the form of 1 cm diameter bar and Inconel®MA956HT as 1 cm thick plate; Alloy PM2000 was supplied by Metallwerk Plansee in the form of 3 mm thick plate, which was warm rolled to 0.7 to 1.5 mm thickness. Specimens of ODM751 were cut from a sample of extruded tubing (2.5 cm diam. x 2.5 mm wall) supplied by British Gas plc.

Specimens were cut from the extruded rods of ODS-Fe₃Al either in the form of 1.25 cm diameter x 0.1-0.15 cm thick discs (transverse sections) or as 1 x 2 x 0.15 cm coupons (longitudinal sections). Coupons of similar size and thickness were cut from Kanthal APM and the commercial ODS-FeCrAl alloys. Specimens typically were abraded through 600 grit SiC papers, water washed and then degreased in methanol and acetone; specimens intended for detailed examination of the oxide scales were further polished through 1 µm diamond paste or 0.3 µm alumina. Before exposure, specimens were measured to 0.01 mm using a digital micrometer, and weighed to the nearest 0.01 mg on a Mettler model AG245 balance.

Exposures were made at temperatures of 1000, 1100, 1200, and 1300°C. Isothermal oxidation kinetics were measured using exposures of typically 100 h (some up to 200 h) in dry oxygen in a Cahn Model 1000 microbalance at temperatures in the range 1000 to 1200°C. Specimens were suspended by Pt-Rh wire through a hole drilled in one end, and corrections were made for the effects of wire evaporation. Longer-term exposure tests were made in box and tube furnaces, with individual specimens exposed in lidded, pre-annealed alumina crucibles so that the total oxygen uptake by the alloys (including any spalled oxide) could be measured. No Pt-Rh wire was used, and holes were not drilled in these specimens. Exposures were made for times of 5,000 h and longer, and the specimens were removed for weighing every 100 h (every 500 h at 1000°C). The long cycle times were chosen to provide some comparison to operation in power generation applications. Some of the data presented are from single specimen exposures, and some are from duplicate or triplicate exposures.

RESULTS

Oxidation Kinetics

Isothermal Oxidation

No systematic difference in oxidation rate was found in the oxidation behavior of the three versions of ODS-Fe₃Al. The kinetic curves for isothermal oxidation in oxygen at temperatures from 1000 to 1200°C for the ODS-Fe₃Al alloys are summarized in Fig. 2 using the data for alloy PMWY-2. At all temperatures, the alloys exhibited oxidation kinetics which approximated a parabolic rate law when the data were plotted versus the square root of time [after Pieraggi⁽²⁰⁾].

Parabolic rate constants were derived from the weight gain-root time curves (no attempt was made to force a fit through the origin) and are shown in Table II. Comparison of the kinetic data for specimens of PMWY-2 in the as-extruded and recrystallized conditions indicated no systematic difference in oxidation rates. Similarly, the oxidation kinetics of PMWY-3, which did not recrystallize under any of the exposure conditions, showed no systematic difference from PMWY-2. The data in Table II were used to draw the Arrhenius plot shown in Fig. 3a. Corresponding data for the Kanthal APM and for the ODS FeCrAl alloys exposed in the same tests are listed in Table II. The value for the activation energy for oxidation derived from Fig. 3a for ODS-Fe₃Al was 251 kJ mol⁻¹ (or, when considering the slowest kinetics at each temperature, 204 kJ mol⁻¹). The activation energy for Kanthal APM was 274 kJ mol⁻¹, whereas for the ODS-FeCrAl alloys the energies were lower: MA956, 195 kJ mol⁻¹; MA956HT, 178 kJ mol⁻¹; PM2000, 143 kJ mol⁻¹; and ODM751, 156 kJ mol⁻¹.

Cyclic Oxidation

Figure 4 shows the oxidation kinetics of ODS-Fe₃Al during the 100-hr cyclic exposure tests in air (500-hr cycles at 1000°C) over the temperature range 1000 to 1300°C. At 1000°C, the data are for an earlier ODS-Fe₃Al, FAS3Y (Table I); at the other temperatures most of the data shown are for PMWY-2, since the behavior of alloys PMWY-1, -2, and -3 alloys was very similar. In all cases, the kinetics of Kanthal APM were used for comparison. The curves indicate the specimen weight change and the total weight change (weight of specimen and any spalled scale). While Kanthal APM exhibited a small amount of scale spallation at all temperatures, scale spallation from ODS-Fe₃Al increased with increasing temperature. The kinetic curves at 1300°C (Fig. 4d) give an indication of the relationship between specimen thickness (total Al reservoir) and time to the onset of rapid oxidation (oxidation lifetime) for ODS-Fe₃Al. Comparison of the curves for the 1.36 mm-thick ODS-Fe₃Al specimen and the 1.32 mm-thick APM specimen suggests that the faster rate of Al consumption from ODS-Fe₃Al due to scale spallation, results in an oxidation lifetime of the same order, not greater, than APM at this temperature. For Kanthal APM, essentially no scale spallation was measured up to and beyond the transition to rapid oxidation.

The total weight change data are shown as a function of the square root of time (parabolic plots) in Fig. 5, and the parabolic rate constants derived from the slopes of the curves are listed in Table II. Data for FAS3Y included in Fig. 5b indicate that it exhibited faster oxidation kinetics than PMWY-2 and -3 after approximately 600 hr. At 1300°C, after a short period of nominally parabolic oxidation, the oxidation rate of all the ODS-Fe₃Al alloys increased significantly. In these cases, the parabolic rate constants reported in Table II are for the early stages of cyclic oxidation. The value for the activation energy for cyclic oxidation, derived from the Arrhenius plot in Fig. 3b for ODS-Fe₃Al, was 423 kJ mol⁻¹ (or, for the slowest kinetics at each temperature, 364 kJ mol⁻¹), noticeably higher than for the isothermal data. The corresponding values for Kanthal APM and the ODS FeCrAl alloys (fit to all data) were 317 and 277 kJ mol⁻¹, respectively.

Oxide Scale Morphologies

Detailed examination of the scale morphologies on ODS-Fe₃Al was made on specimens exposed isothermally. Only a limited examination was made of the scales formed on the specimens exposed to thermal cycling, because of the complex morphologies resulting from spalling and scale regrowth.

Isothermal Oxidation at 1100°C

Figures 6a-d show the morphology of the scale formed on the fine-grained (not recrystallized) alloy PMWY-1 after 119 hr of exposure. In plan view, the scale appeared macroscopically smooth and flat, with a uniformly small grain size (Fig. 6a). In cross section the scale was uniform in thickness and the metal-oxide interface appeared essentially flat (Fig. 6b), although in some locations the interface was found to be undulating on a microscopic scale with a typical amplitude of 3 to 10 μm (Figs 6c, d). There was evidence of cracking of the oxide (similar to the shear-type cracking modeled by Evans⁽²¹⁾ and others) over some of these undulations, as shown in Fig. 6c. There were also occasional larger undulations (amplitude 8-10 μm), over which the local scale had been completely detached by the formation of such shear cracks, Fig. 6d. The length (some 30 μm) of oxide detached in this way is consistent with the overall macroscopic observation that spallation of oxide occurs from Fe_3Al in the form of 'fine dust'⁽¹⁰⁾. The bright-appearing features (arrows) in the scales in the cross sections shown in Figs 6c and d were shown by electron probe microanalysis to be yttrium-rich (likely YAG) and to be associated with the oxide grain boundaries. There was slight thickening of the scale associated with these grain boundaries (see, for instance, the metal-oxide interface in these areas in Fig. 6c), suggesting possibly increased oxygen transport.

In areas where the scale had spalled on cooling, the bare alloy surface exhibited the familiar oxide 'footprints'^(22,23), Fig. 6e (for large-grained PMWY-2 after 100 hr). The fracture section of the oxide on this same specimen showed that the scale was essentially one grain thick, consisting of large, columnar grains with a few finer grains at the oxide-gas interface (Fig. 6f) typical for RE-doped alumina^(8,24).

The grinding lines from surface preparation were plainly visible in the relatively flat oxide on recrystallized (large-grained) PMWY-2 after isothermal exposure for 100 hr at 1100°C (Fig. 7a), and the outer oxide surface was uniformly fine-grained (finer than on PMWY-1). At this temperature, scale spallation typically was observed in only one or two areas, which formed a 'trench' across the specimen width, as exemplified on fine-grained PMWY-3 after 116 hr at 1100°C (Fig. 7b). The alloy surface was visible at the bottom of the trench (Fig. 7c). In cross section, the adherent scale consisted of columnar grains which extended from the alloy surface to near the oxide-gas interface, and a fine-grained outer layer.

Isothermal Oxidation at 1200°C

After 120 hr exposure there were numerous areas of scale spallation on the surface of the fine-grained PMWY-1 (Fig. 8a), with buckles and spallation apparently initiating along polishing scratches in the alloy surface. The outer surface of the adherent oxide was undulating (Fig. 8b), compared to the macroscopically flat surface at 1100°C. The grain size at the outer surface of the scale was uniform and larger than at 1100°C. In cross section, the 8 μm -thick scale was essentially columnar-grained and one grain thick^(8,24). It appeared that this scale had been in good contact with the substrate at temperature, since areas of alloy surface from which spallation had occurred exhibited only small interfacial voids, very different to the numerous interfacial voids observed on the earlier ODS- Fe_3Al alloy, FAS3Y⁽¹⁶⁾. Spalling appeared to have occurred only on cooling at the end of the test.

The path followed by scale spallation was dependent on the alloy surface finish. Whereas undulations in the scale and areas of spallation that aligned with polishing lines on the surfaces of specimens oxidized with a 600 grit surface finish, on highly-polished specimens (0.3 μm alumina) the spalled areas occurred in a non-aligned, random pattern similar to those reported by Evans⁽²⁵⁾, as shown in Fig 9a for PMWY-2 after 100 hr. Metallographic cross sections showed the adherent scale to be uniform in thickness, but that there were obvious undulations in the alloy-oxide interface of the same order of length as those observed in the scale topography. Fracture cross sections of the scales showed the characteristic columnar grain structure. The alloy surface beneath spalled areas again showed footprints of the oxide grains, indicating that the scale had been in excellent contact with the substrate before spallation, together with small interfacial voids at the scale grain boundaries, often associated with oxide grain boundary triple points (Fig. 9b).

Isothermal Oxidation at 1300°C

Fig. 10a shows pronounced macroscopic undulations in the oxide, some with obvious cracking, on the surface of a highly-polished specimen of PMWY-1 after 100 hr exposure. Metallographic cross sections showed that undulations were present in the metal-oxide interface, that the scale was essentially uniform in thickness and that, in some cases, there were cracks in the outer surface of the oxide (Fig. 10b) associated with undulations in the alloy surface. In some areas, outward buckling of the oxide was associated with extreme, localized outward extrusion of the substrate alloy (Fig. 10c); these are features that have not yet been considered in modeling of scale spallation processes. In areas where complete scale spallation had occurred, typical oxide grain 'footprints' were observed along with voids at the locations corresponding to the grain boundaries in the oxide, as at 1200°C. These voids appeared to be no larger or numerous than at 1200°C (Fig. 10d), suggesting that they are not Kirkendall voids, but are probably related to gas adsorbed on the alloy powder during processing. A fracture cross section of the adherent oxide showed the typical elongated columnar grains throughout most of its thickness and some void formation in the outer regions of the scale Fig. (10e); the arrow indicates an interfacial void.

FeCrAl Alloy Kanthal APM

The scales formed on Kanthal APM after isothermal exposures were generally uniform in thickness, the metal-oxide interfaces were macroscopically flat, and very little spallation occurred (Fig. 11a, after 200h isothermal exposure at 1200°C). The majority of the scale thickness consisted of large, columnar grains, with smaller, more equiaxed grains near the oxide-gas interface (Fig. 11b), indicating that the major mode of scale growth was by inward oxygen transport⁽⁸⁾. Details of these morphologies, and of those formed on the ODS-FeCrAl alloys for which kinetic data were used for comparison in this paper, are discussed elsewhere^(12,16). However, after exposure to more thermal cycles, the metal-oxide interface was observed to develop significant undulations in some areas, as indicated in Fig. 11c, for a specimen that was exposed for 20 x 100h cycles at 1100°C. Fig. 11d is a plan view of these features, with obvious cracking at the tips of several of the undulations, and Fig. 11e is a metallographic cross section through such an undulation. Significant localized outward extrusion of the substrate alloy caused the oxide buckling, in a manner very similar to that observed on ODS-Fe₃Al after isothermal exposure at 1300°C.

Coefficient of Thermal Expansion

Thermal expansion measurements were made on ODS-Fe₃Al (PMWY-2) over the temperature range 25 to 1200°C using a Theta Industries dual push-rod differential dilatometer. The methodology used employs high-density alumina push rods and sample holder in a horizontal configuration, as described in detail elsewhere⁽²⁶⁾. The temperature dependence of the mean coefficient of thermal expansion of ODS-Fe₃Al is shown in Fig. 12, in comparison to literature values for MA956⁽²⁷⁾, PM2000⁽²⁸⁾, and polycrystalline alumina⁽²⁹⁾. It is clear that the CTE of ODS-Fe₃Al is significantly greater than for the ODS-FeCrAls, and that it has a quite different temperature dependence as a result of the DO₃-to-B2, and B2-to- (disordered) phase changes which occur at 533°C and 821°C, respectively. The CTE between ODS-Fe₃Al and polycrystalline alumina, shown in Fig. 13, indicates that a maximum (approximately 12 x 10⁻⁶/°C) exists at approximately 900°C; this value is some 2.4 times that for the ODS-FeCrAls.

DISCUSSION

Over the temperature range 1000 to 1300°C, the isothermal oxidation rate of ODS-Fe₃Al (measured from 100 h exposures) was very similar to that of Kanthal APM and the commercial ODS FeCrAl alloys, but became increasingly higher with temperature increases above 1100°C. ODS-Fe₃Al formed an -alumina scale (as did the FeCrAl alloys) that exhibited all of the morphological features expected from RE-doping: columnar-grained oxide essentially one grain thick; no external growth of alumina needles; essentially no porosity at the metal-oxide interface; and a macroscopically-flat metal-oxide interface^(8,24,30). The activation energy for the oxidation of ODS-Fe₃Al (calculated from isothermal data, 100 h exposures) was 251 kJ mol⁻¹, very similar to that reported by Pettit⁽³¹⁾ (272 kJ mol⁻¹) for the isothermal oxidation of a cast Ni-25 wt% Al alloy that forms an exclusively alumina scale. The reported apparent activation energy for oxygen diffusion in Al₂O₃ (bulk diffusion, single

crystal data) ranges from 590 to 665 kJ mol⁻¹⁽³²⁾; based on sintering kinetics, Coble⁽³³⁾ reported a value of 690 kJ mol⁻¹ for polycrystalline material. Activation energies for aluminum diffusion calculated from creep data range from 476 to 573 kJ mol⁻¹ for polycrystalline alumina⁽³⁴⁾. The fact that the rate-controlling process in the isothermal oxidation of ODS-Fe₃Al involves an activation energy approximately one half of these values, while the oxide morphology indicates growth by predominantly oxygen transport, strongly suggests that transport is operating along short circuit paths—oxide grain boundaries. This is probably a reflection of the yttrium ions incorporated in the scale to promote the development of columnar oxide grain boundaries. The observed segregation of yttrium to the oxide grain boundaries in ODS-Fe₃Al⁽¹¹⁾ and similar ODS systems⁽³⁵⁾ will certainly modify the chemistry and properties of these regions and significantly modify their transport properties. The fact that the activation energy for isothermal oxidation of ODS-Fe₃Al (predominantly grain boundary transport of oxygen ions) and RE-free cast Ni-25Al⁽³¹⁾ (grain boundary transport of both oxygen and aluminum ions) was essentially the same suggests that the activation energy of the transport process is, in fact, not affected by the yttrium segregation, or that the activation energies for grain boundary transport of oxygen and aluminum ions are similar. The still lower activation energies measured for the ODS FeCrAl alloys (143 to 195 kJ mol⁻¹) suggest that similar short circuit diffusion processes are involved in these alloys. Activation energies in the range 100 to 240 kJ mol⁻¹ have, in fact, been measured for (bulk) oxygen diffusion in alumina under conditions where diffusion was enhanced by microwave heating⁽³²⁾.

The oxidation rates derived from long-term cyclic exposures were slower than the shorter-term isothermal oxidation rates, but were similar for the ODS-Fe₃Al, Kanthal APM, and the ODS-FeCrAl alloys up to 1100°C. The activation energy calculated from these data (100h cycles, several thousand-hour exposures) was significantly higher than from the short-term, isothermal exposures (Fig 3). However, there is little value in trying to attribute much mechanistic significance to the higher value for activation energy (423 vs. 251 kJ mol⁻¹) calculated from the cyclic oxidation data since the specimens in these tests experienced significant scale spallation and regrowth. Nevertheless, these data represent long-term oxidation behavior that is important for oxidation life prediction. The overall oxidation rate expression for ODS-Fe₃Al for the temperature range 1000 to 1300°C, based on long-term cyclic oxidation exposures in air, is:

$$k_p = 7.5 \times 10^3 e^{-50,830/T}$$

where k_p is the parabolic rate constant, in g²cm⁻⁴s⁻¹, and T is the oxidation temperature in degrees K.

A major characteristic of the cyclic oxidation behavior of ODS-Fe₃Al was the tendency for significantly more scale spallation to occur than for FeCrAl alloys. For the most part, the adherence of the oxide to ODS-Fe₃Al appeared to be tenacious but, with increasing time at temperature (especially at 1100°C and higher), spallation of small fragments of scale occurred in amounts that increased with increasing time and temperature. Hence, the overall rate of aluminum consumption was higher compared to ODS-FeCrAl. Spallation from ODS-Fe₃Al became measurable at weight gains of approximately 1.5 mg/cm², equivalent to a scale thickness of 8 μm. As discussed elsewhere⁽³⁶⁾, the scale thickness at which spallation becomes obvious appears to depend on the frequency of thermal cycling, so this should not be considered a limiting scale thickness for other conditions of exposure.

Scale spallation from ODS-Fe₃Al appeared to result from cracking associated with undulations in the alloy-oxide interface. Such undulations were small at 1000 and 1100°C but increased in size at 1200°C and were very large at 1300°C. Up to 1100°C, the oxide layer cracked and was lost from the tops (convex regions) of the surface undulations, and scale spallation occurred in only one or two locations on any given surface. The ‘trenches’ observed at 1100°C were possibly the remnants of large buckles in the oxide that spalled on cooling. At 1200 and 1300°C it appeared that some of the stress between the oxide and substrate had been accommodated by significant deformation of the substrate. Obvious through-cracking was observed in the scale at the tops of the undulations, and in some of these regions shear cracks (parallel to the alloy-oxide interface) were present at 1200°C, similar to those described by Evans⁽²¹⁾. Apparently, at 1300°C the stresses generated were sufficient to cause gross local deformation of the substrate and, although the oxide appeared to have excellent adherence to the substrate, the out of plane tensile component of the compressive thermal stress caused by the surface undulations resulted in cracking and scale loss. Observations of the scales

formed on Kanthal APM (and on the commercial ODS-FeCrAls⁽¹⁶⁾) indicated that, although similar undulations were sometimes present in the metal-oxide interfaces, when they did occur they were typically much smaller than on ODS-Fe₃Al after similar exposures.

The basic driving forces for scale spallation are stresses resulting from the accommodation of the increased volume of oxide compared to the alloy from which it was formed (Pilling-Bedworth forces⁽³⁷⁾), and thermally-induced stresses resulting from the difference in the coefficient of thermal expansion of the oxide and the alloy substrate. The stresses from the former source increase with increasing scale thickness (time at temperature), but they may be relieved to some extent by deformation of the substrate (or oxide) at temperature. The macro yield and tensile strengths of ODS-Fe₃Al are very similar to those of the ODS-FeCrAl alloys at temperatures up to 1100°C. The creep strength of ODS-Fe₃Al is similar to that of MA956, somewhat less than for PM2000 in the range 800 to 1100°C^(13,27, 28), and would be expected to be greater than for Kanthal APM. Hence, it would be expected that, for a given rate of scale growth, relaxation of the Pilling-Bedworth stresses would occur at a similar or greater rate on Kanthal APM than on ODS-Fe₃Al or ODS-FeCrAls.

In contrast to the Pilling-Bedworth stresses, those from the CTE mismatch develop during the cooling cycle of the oxidation exposure. It is clear that the CTE of ODS-Fe₃Al is significantly greater than for the ODS-FeCrAls. The stress (σ_{ox}) resulting from the different coefficients of thermal expansion of the oxide (α_{ox}) and alloy (α_{alloy}) can be estimated⁽³⁸⁾ from:

$$\sigma_{ox} = -E_{ox} T(\alpha_{alloy} - \alpha_{ox})/(1-\nu)$$

where E_{ox} and ν are the elastic modulus (360 GPa⁽³⁹⁾) and the Poisson's ratio of the oxide of the oxide (estimated to be 0.3), respectively. For the case of a ODS-Fe₃Al specimen cooled from 1300°C to 25°C the estimated compressive stress developed is 7.6 GPa,. Recent measurements have indicated a residual compressive stress of 9 GPa in the scale formed on this alloy after exposure for 20 h at 1200°C⁽⁴⁰⁾, which is not surprising given the large CTE. This stress level suggests a corresponding strain in the scale of approximately 2 percent and, since a strain of only 0.1 to 0.2 percent is sufficient to fail an alumina scale in compression or tension⁽⁴¹⁾, it is clear that conditions for scale failure exist. Hence, the large CTE mismatch between ODS-Fe₃Al and alumina appears to be the major inherent reason for the increased tendency for scale spallation of this alloy.

It is generally accepted that there are two main sources for the initiation of scale spallation: void formation at the metal-oxide interface, as seen in Figs. 9b, 10d and e, and scale lifting due to out-of-plane stresses or surface discontinuities. The interfacial voids observed on ODS-Fe₃Al appeared to be very small compared to the voids usually associated with scale spallation, and do not appear to grow with continued oxidation. The source of the interfacial voids in RE-doped alloys forming alumina scales is not obvious, since essentially all of the scale formation takes place at the metal-oxide interface via oxygen anion transport through the scale. There does not appear to be an obvious outward flux of Al cations through the scale in the commonly-accepted sense that would be a source of vacancies that could condense into voids. Since the transfer of Al ions into the alumina lattice will initiate transport of Al from the alloy bulk and a compensating movement of Fe away from the interface, one possibility is that the interfacial voids result from the Kirkendall voids due to Fe diffusion. No obvious Kirkendall voids resulting from Al diffusion were observed at the temperatures studied. Although small voids were commonly observed on the surface of ODS-Fe₃Al, they did not appear to increase in size or population with increasing exposure time and did not appear to be associated with scale growth/adhesion. Similar voids have been observed on other alumina scale-forming ODS alloys^(42,43) and are possibly due to gas entrapped in the alloy structure during powder processing.

Hence, the larger CTE mismatch between ODS-Fe₃Al and alumina appears to be a major reason for the increased tendency for scale spallation of this alloy. It is apparent that this CTE mismatch problem will not be solved by small modifications of the alloy composition. Minimization of the growth rate of the oxide scale is, nevertheless, a worthwhile goal for maximizing its service lifetime. It is also important to have an accurate knowledge of the temperature dependence of oxidation in environments of interest to allow calculation of the rate of consumption of Al, and of the minimum Al level to which the substrate can be depleted before non-protective behavior ensues. Oxidation

lifetime models, such as that due to Quadackers, et al.⁽¹⁴⁾ and Bennett et al.,⁽¹⁵⁾ equate the oxidation lifetime (t_b) to the time required to deplete the alloy Al reservoir from the initial level (C_o) to some critical level (C_b), where the Al is consumed in the formation of the protective oxide scale:

$$t_b = [4.44 \times 10^{-3} \cdot (C_o - C_b) \cdot \rho \cdot d/k]^{1/n}$$

where ρ is the density of the alloy, d the section thickness, k is the oxidation rate constant, T is the oxidation temperature, n is the time-dependence exponent (0.5 for parabolic oxidation behavior), and R is the gas constant. Clearly, t_b will be increased by increasing C_o and decreasing both C_b and k .

SUMMARY AND CONCLUSIONS

ODS-Fe₃Al reliably forms an exclusively alumina scale and exhibits an expected slow rate of isothermal oxide scale growth over the temperature range 1000 to 1300°C. The rate of aluminum consumption from the alloy appears to be very similar to those for Kanthal APM and the ODS-FeCrAl alloys up to 1100°C, but at higher temperatures an increased tendency for scale spallation from ODS-Fe₃Al increases the Al consumption rate. The major reason for the greater tendency for scale spallation compared to the FeCrAl alloys appears to be a significantly higher coefficient of thermal expansion for ODS-Fe₃Al, which leads to development of higher stresses between the alloy and the thermally-formed oxide scale. Even though the inherent adherence of the oxide scale to ODS-Fe₃Al appears to be excellent, the stress generated by the coefficient of thermal expansion mismatch appears sufficient to lead to deformation of the alloy surface resulting in scale spallation from out-of-plane tensile stress situations. Although similar metal-oxide features also are observed on Kanthal APM and ODS-FeCrAls, they typically are much less developed for a given exposure.

Given the source of the increased stress at the metal-oxide interface compared to Kanthal APM and the ODS-FeCrAls, there appears to be no obvious route to improving the scale spallation behavior of ODS-Fe₃Al. Optimization of the effects of minor alloying additions to ensure that the alumina scale on ODS-Fe₃Al exhibits all the attributes of a practically 'ideal' alumina scale⁽⁸⁾ including the minimum possible oxide growth rate remains an important goal. Nevertheless, the large aluminum reservoir of ODS-Fe₃Al still provides the potential for achieving greater oxidation-limited lifetimes to the ODS-FeCrAl alloys. Hence, accurate knowledge of the temperature-dependence of its oxidation rate, together with a mechanistic description of the mode of scale loss, remain important roles in developing a reliable prediction of lifetimes.

ACKNOWLEDGMENTS

This research was sponsored by the Fossil Energy Advanced Research and Technology Development (AR&TD) Materials Program, U.S. Department of Energy, under contract DE-AC05-84OR21400 with Lockheed Martin Energy Research Corp., Inc. Thanks are due to Dr. G. Smith of INCO, Dr. D. Sporer of Metallwerk Plansee, and Mr. Q. J. Mabbutt of British Gas plc. for supplying samples of ODS-FeCrAl alloys. We would like to also acknowledge the contributions of colleagues at the Oak Ridge National Laboratory: Dr. J. H. DeVan for helpful discussions; Mr. L. D. Chitwood, G. W. Garner, and Mr. M. Howell who were responsible for the oxidation testing; and Mr. W. Porter for measurement of the coefficients of thermal expansion of the alloys.

REFERENCES

1. M.P. Brady, B.A. Pint, P.F. Tortorelli, I.G. Wright, and R.J. Hanrahan, Jr., in: *Corrosion and Environmental Degradation of Material*, Volume Editor: M. Schütze (Volume 19 of the series: *Materials Science and Technology*, Series Editors: R.W. Cahn, P. Haasen, E.J. Kramer, Wiley-VCH, Weinheim, Germany, 2000).
2. W. C. Hagel, *Corrosion*, 21, 316-326 (1965).
3. P. Tomaszewicz and G. R. Wallwork, *Reviews of High-Temperature Materials*, 4, 75-105 (1978).
4. R. Prescott and M. J. Graham, *Oxidation of Metals*, 38, 73-87 (1992).
5. P. F. Tortorelli and J. H. DeVan, *Materials Science and Engineering*, A153, 573-577 (1992).
6. P. F. Tortorelli and K. Natesan, *Materials Science and Engineering*, A258, 115-125 (1998).
7. M. Sakiyama, P. Tomaszewicz, and G. R. Wallwork, *Oxidation of Metals*, 13, 311-330 (1979).

8. B. A. Pint, pp. 74-85 in *Fundamental Aspects of High Temperature Corrosion*, D.A. Shores, R.A. Rapp, and P.Y. Hou, Editors (The Electrochemical Society, Pennington, NJ, 1997).
9. D. Renusch et al., *ibid.*, pp. 62-73
10. J. H. DeVan, "Oxidation Behavior of Fe₃Al and Derivative Alloys," Pp. 107-115 in *Oxidation of High-Temperature Intermetallics*, T. Grobstein and J. Doychak, Eds. (The Minerals, Metals & Materials Society 1988).
11. B. A. Pint, P. F. Tortorelli, and I. G. Wright, *Werkstoffe und Korrosion*, 47, 663-674 (1996).
12. B. A. Pint, P. F. Tortorelli, and I. G. Wright, *Materials at High Temperatures*, 16 (1), 1-13 (1999).
13. I. G. Wright, B. A. Pint, P. F. Tortorelli, and C. G. McKamey, pp. 359-371 in *Proc. Tenth Annual Conference on Fossil Energy Materials*, Oak Ridge, Tennessee (ORNL Report No. ORNL/FMP-96/1, CONF-9605167, 1996).
14. W. J. Quadackers, K. Bongartz, F. Schubert, and H. Schuster, Pp. 1533-1542 in *Materials for Advanced Power Engineering 1994*, D. Coutsouradis, et al., Eds., (Kluwer Academic Publishers, 1994).
15. M. J. Bennett, R. Perkins, J. B. Price, and F. Starr, Pp. 1553-1562 in *Materials for Advanced Power Engineering 1994*, D. Coutsouradis, et al., Eds. (Kluwer Academic Publishers, 1994).
16. B. A. Pint, P. F. Tortorelli, and I. G. Wright, *Oak Ridge National Laboratory report, in preparation, 2000.*
17. J. S. Benjamin, *Metallurgical Transactions*, 1, 1-9 (1970).
18. J. H. DeVan, P. F. Tortorelli, M. J. Bennett, pp. 309-320 in *Proc. Eighth Annual Conference on Fossil Energy Materials*, Oak Ridge, Tennessee (CONF-9405143; ORNL/FMP-94/1, 1994).
19. I. G. Wright, B. A. Pint, P. F. Tortorelli, and C. G. McKamey, pp. 265-278 in *Proc. Eleventh Annual Conference on Fossil Energy Materials*, Knoxville, Tennessee (ORNL Report No. ORNL/FMP-97/1, CONF-9705115, 1997).
20. B. Pieraggi, *Oxidation of Metals*, 27 (3/4), 177-185 (1987).
21. H. E. Evans, *Materials at High Temperatures*, 12, 219-27 (1994).
22. J. L. Smialek, *Metallurgical Transactions*, 9A, 309-20 (1978).
23. J. D. Kuenzly and D. L. Douglass, *Oxidation of Metals*, 8, 139-178 (1974).
24. F. A. Golightly, F. H. Stott and G. C. Wood, *Journal of the Electrochemical Society*, 126, 1035-42 (1979).
25. A. G. Evans, M. Y. He and J. W. Hutchinson, *Acta Materialia*, 45, 3543-54 (1997).
26. W. D. Porter, and P. J. Maziasz, *Scripta Metallurgica et Materialia*, 29, 1043-1048 (1993).
27. J. Fischer, J. J. deBarbadillo, and M. J. Shaw, pp. 79-87 in *Structural Applications of Mechanical Alloying*, F. H. Froes and J. J. deBarbadillo, Eds. (ASM International, 1990).
28. Materials Data Sheet: *ODS Superalloy PM2000*, Metallwerk Plansee GmbH/Lechbruch, Feb 1993.
29. Y. S. Touloukian, R. K. Kirby, R. E. Taylor, and T. Y. R. Lee, *Thermal Expansion—Nonmetallic Solids, Vol. 13 of Thermophysical Properties of Matter* (IFI/Plenum, New York, 1970).
30. B. A. Pint, Garratt-Reed, L. Hobbs, *Materials at High Temperatures*, 13, 3-16 (1995).
31. F. S. Pettit, *Transactions of the American Institute of Mechanical Engineers*, 239, 1297 (1967).
32. M. A. Janney, H. D. Kimrey, W. R. Allen, and J. O. Kiggans, *Journal of Materials Science*, 32, 1347-1355 (1997).
33. R. L. Coble, *Journal of the American Ceramics Society*, 41 (2), 55-62 (1958).
34. A. E. Paladino and R. L. Coble, *Journal of the American Ceramics Society*, 46 (3), 133-136 (1963).
35. B. A. Pint and K. B. Alexander, *Journal of the Electrochemical Society*, 145, 1819-29 (1998).
36. B.A. Pint, P.F. Tortorelli, and I.G. Wright, Pp. 111-32 in *Cyclic Oxidation Testing of High-Temperature Materials*, M. Schütze and W. J. Quadackers, Eds. (European Federation of Corrosion Publication 27, IOM Communications, London, 1999).
37. N. B. Pilling and R. E. Bedworth, *Chemical and Metallurgical Engineering*, 27 (2), 72-74 (1922).
38. M. Schütze, Chapter 4.2 in *Protective Scales and Their Breakdown*, Edited by D. R. Holmes, Translated by R. B. Waterhouse (The Inst. of Corrosion and Wiley Series on Corrosion and Protection, John Wiley & Sons Ltd., 1997).
39. J. A. Haynes, Oak Ridge National Laboratory, private communication (1999).
40. M. Lance and B. A. Pint, Oak Ridge National Laboratory, unpublished work (1999).
41. S. R. J. Saunders, M. E. Evans, M. Li, D. D. Gohil, and S. Osgerby, *Oxidation of Metals*, 48 189-200 (1997).
42. B. A. Pint, *Oxidation of Metals*, 48, 303-28 (1997).
43. B. A. Pint, *Oxidation of Metals*, 49 531-60 (1998).

FIGURE CAPTIONS

- Figure 1. Typical microstructures of ODS-Fe₃Al alloys: etched, longitudinal cross sections (a) as-extruded, PMWY-1; (b) after recrystallization, PMWY-2
- Figure 2. Summary of isothermal oxidation kinetics of ODS-Fe₃Al (PMWY-2).
- Figure 3. Temperature-dependence of the ODS-Fe₃Al alloys in (a) isothermal exposures, and (b) cyclic exposures (100-500-h cycles).
- Figure 4. Oxidation kinetics of ODS-Fe₃Al and ODS-FeCrAl (APM) in cyclic oxidation tests, indicating extent of scale spallation, at (a) 1000°C (b) 1100°C (c) 1200°C and (d) 1300°C; the original specimen thicknesses are indicated.
- Figure 5. Summary of cyclic oxidation kinetics of ODS-Fe₃Al based on total weight gains (total oxygen consumption) at: (a) 1000°C; (b) 1100°C; (c) 1200°C; and (d) 1300°C. Data for Kanthal APM are included for comparison.
- Figure 6. Scale formed on ODS-Fe₃Al alloy after isothermal exposure at 1100°C: (a) plan view, and (b)-(d) metallographic cross sections of PMWY-1 (fine-grained, not recrystallized) after 119 hr; arrows indicate Y-rich particles in the scales; (e) alloy surface beneath spalled scale, and (f) fracture section of adherent scale on PMWY-2 (recrystallized, large-grained) after 100 hr.
- Figure 7. Plan views of scale formed on ODS-Fe₃Al alloy after isothermal exposure at 1100°C: (a) recrystallized (large-grained) PMWY-2 after 100 hr; (b) fine-grained alloy PMWY-3 after 116 hr (c) detail of (b) showing spallation trench.
- Figure 8. Topography of scale formed on fine-grained (not recrystallized) alloy PMWY-1 after 120 hr at 1200°C: (a) areas of spallation, (b) undulations in scale.
- Figure 9. PMWY-2 after 100 hr of isothermal exposure at 1200°C: (a) plan view of scale on large-grained alloy; (a) spallation, (b) alloy surface beneath spalled scale.
- Figure 10. Scale formed on alloy PMWY-1 after 100 hr of isothermal exposure at 1300°C: (a) plan view showing undulations in the oxide and cracking, (b) metallographic cross section through an area of undulation, (c) metallographic cross section through buckled scale, (d) alloy surface beneath spalled scale, and (e) fracture section; arrow indicates an interfacial void
- Figure 11. Scales formed on FeCrAl alloy APM after at exposure at 1200°C: (a) metallographic cross section and (b) fracture cross section after 200 h of isothermal exposure; (c) and (e) metallographic cross sections and (d) plan view after 20 x 100 h cycles at 1100°C.
- Figure 12. Comparison of mean coefficients of thermal expansion of ODS alloys with that of alumina.
- Figure 13. Variation with temperature of the difference between coefficients of thermal expansion of ODS-Fe₃Al and alumina.

Table I. Chemical compositions of alloys studied (weight percent)

| Alloy | Fe | Ni | Cr | Al | Mn | Cu | Ti | Si | P | C | O | N ^a | S ^a | RE ^b |
|---------|-------|------|-------|-------|------|------|-------|------|--------|------|-------|----------------|----------------|------------------|
| FAS3Y | Bal. | — | 2.25 | 16.3 | 0.15 | — | 0.07 | 0.10 | — | 0.03 | 2.03 | — | 61 | 0.47 |
| PMWY-1 | 81.68 | 0.05 | 2.61 | 14.67 | 0.04 | 0.01 | 0.01 | 0.04 | 0.008 | 0.06 | 0.323 | 968 | 22 | 0.48 |
| PMWY-2 | 81.45 | 0.03 | 2.33 | 15.36 | 0.03 | 0.01 | <0.01 | 0.03 | 0.008 | 0.04 | 0.207 | 1024 | 20 | 0.50 |
| PMWY-3 | 81.54 | 0.03 | 2.33 | 15.43 | 0.02 | 0.01 | <0.01 | 0.04 | 0.008 | 0.03 | 0.145 | 44 | 16 | 0.51 |
| APM | 73.31 | — | 20.42 | 5.54 | 0.08 | — | 0.03 | 0.23 | — | 0.03 | 0.05 | — | 10 | 0.1 ^c |
| MA956 | Bal. | — | 19.22 | 4.32 | — | — | 0.36 | — | — | 0.01 | 0.20 | — | 110 | 0.63 |
| MA956HT | 71.19 | 0.11 | 21.66 | 5.77 | 0.06 | — | 0.40 | 0.05 | — | 0.03 | — | 288 | 50 | 0.38 |
| PM2000 | 74.58 | 0.01 | 18.92 | 5.10 | 0.11 | 0.01 | 0.45 | 0.04 | <0.002 | 0.01 | 0.248 | 28 | 21 | 0.37 |

a: ppmw

b: as Y₂O₃

c: as Zr

Table II. Summary of parabolic rate constants (10⁻¹³ g²cm⁻⁴s⁻¹)

| Alloy | 1000°C | | 1100°C | | 1150°C | 1200°C | | 1300°C |
|--------|-------------------------|----------------------------|------------|---------------|------------|------------|---------------|---------------|
| | <i>iso</i> ^a | <i>cyclic</i> ^b | <i>iso</i> | <i>cyclic</i> | <i>iso</i> | <i>iso</i> | <i>cyclic</i> | <i>cyclic</i> |
| PMWY-1 | 1.7-6.6 | — | 11 | — | 22-25 | 44-46 | — | 2,732 |
| PMWY-2 | 3.0 | 0.33 | 8.7-20 | 7.1-12 | 35-14 | 19-73 | 50-255 | 217-1537 |
| PMWY-3 | 1.9-3.2 | — | 19 | 2.5 | 43 | — | — | 186-1677 |
| APM | 1.9 | 0.47 | 13-3.3 | 7.8-8.2 | 53-4.6 | 60-30 | 20-41 | 238-775 |
| ODM751 | 2.7-0.15 | 0.22 | 20 | 5.4-6.8 | — | — | 140-135 | 113-115 |
| MA956 | 1.5-4.5 | — | — | 8.8 | — | 34-41 | 35-84 | 587 |
| MA956H | 5.0-0.12 | — | 37-8.0 | 9.0-9.2 | 108-9.4 | 43-67 | — | 146-351 |
| PM2000 | 7.1-0.07 | 0.72 | 11-15 | 8.1-9.2 | — | 44 | 26-75 | 95-453 |

a: kinetics derived from weight gain-square root time plots of data from Cahn microbalance.

b: kinetics derived from weight gain-square root time plots of data from intermittent weighing of specimens oxidized in individual crucibles.

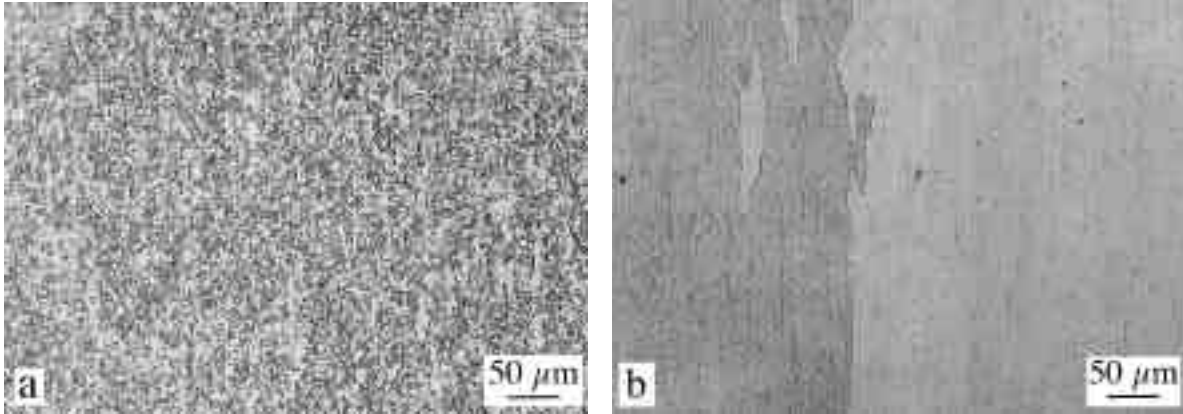


Figure 1. Typical microstructures of ODS-Fe₃Al alloys: etched, longitudinal cross sections (a) as-extruded, PMWY-1; (b) after recrystallization, PMWY-2

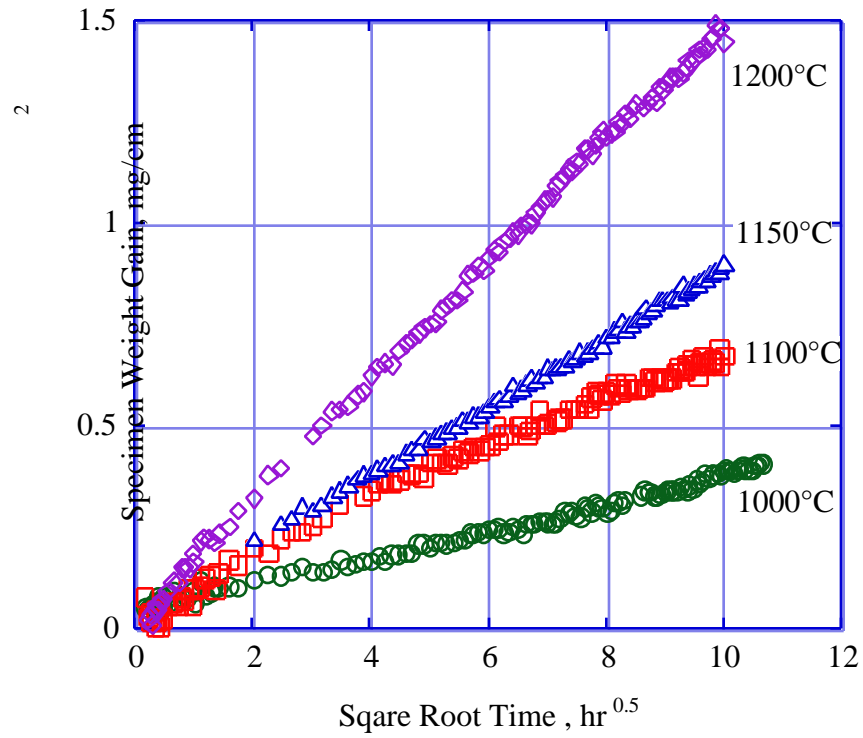


Figure 2. Summary of isothermal oxidation kinetics of ODS-Fe₃Al (PMWY-2).

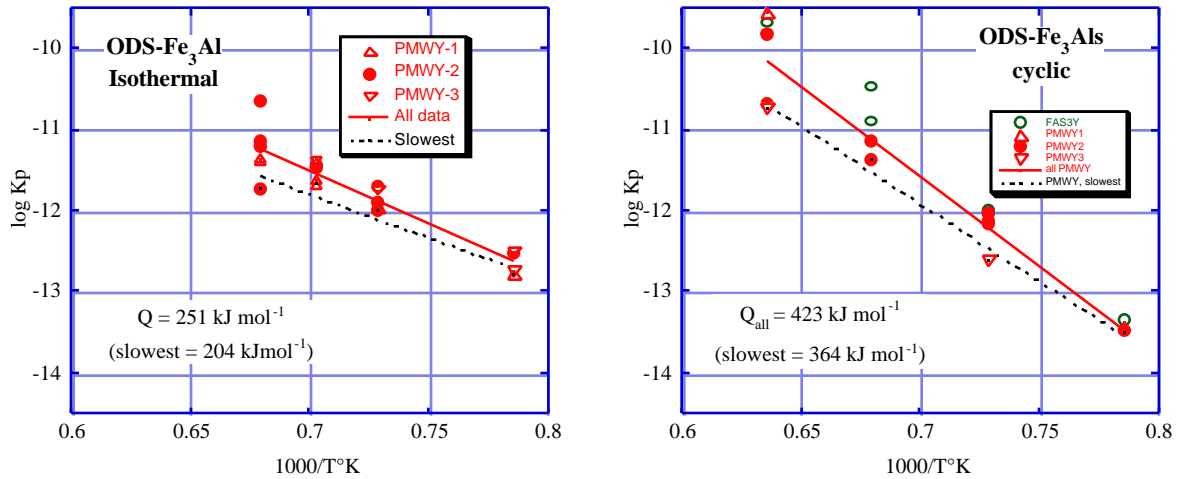


Figure 3. Temperature-dependence of the ODS-Fe₃Al alloys in (a) isothermal exposures, and (b) cyclic exposures (100-500-h cycles).

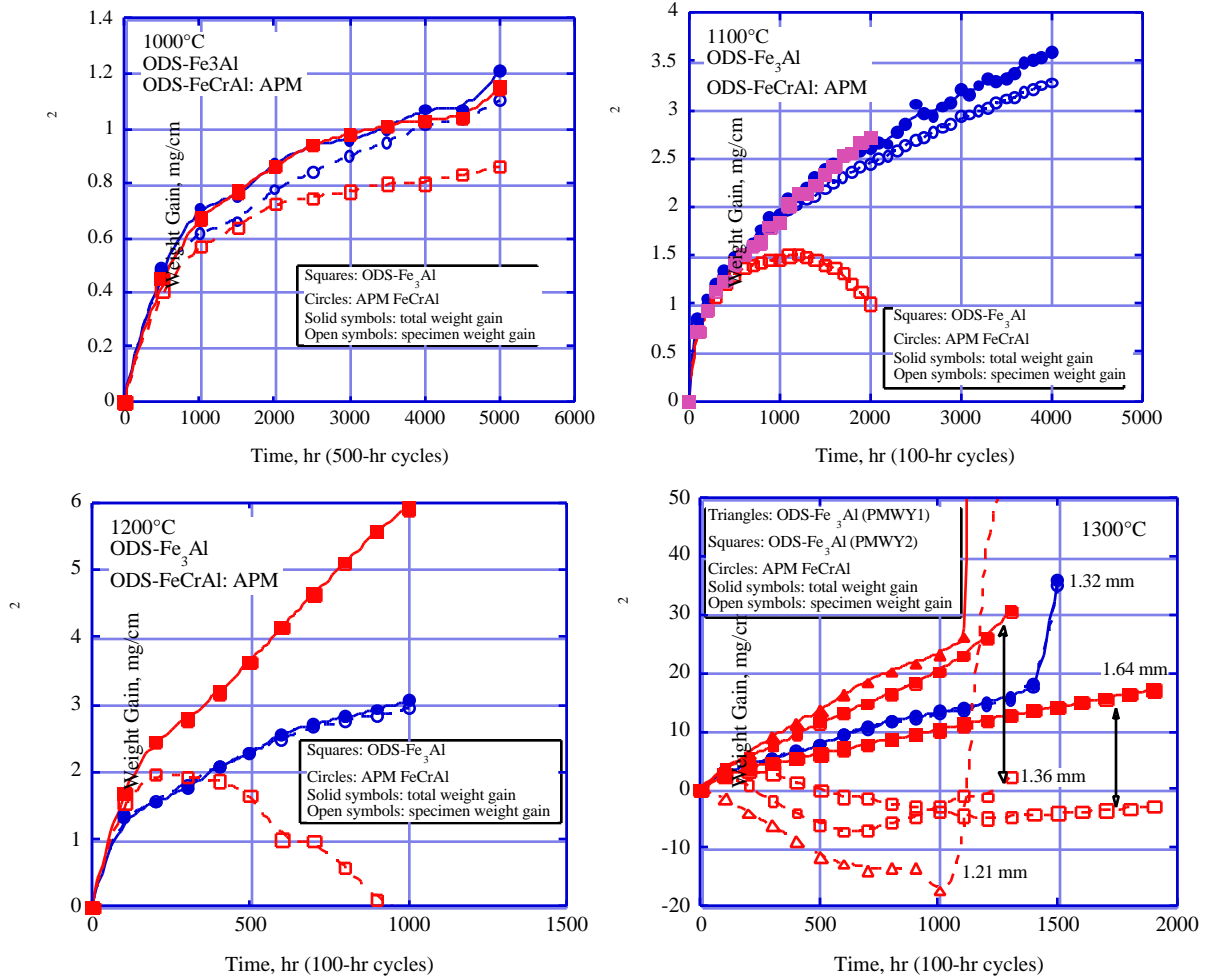


Figure 4. Oxidation kinetics of ODS-Fe₃Al and ODS-FeCrAl (APM) in cyclic oxidation tests, indicating extent of scale spallation, at (a) 1000°C (b) 1100°C (c) 1200°C and (d) 1300°C; the original specimen thicknesses are indicated.

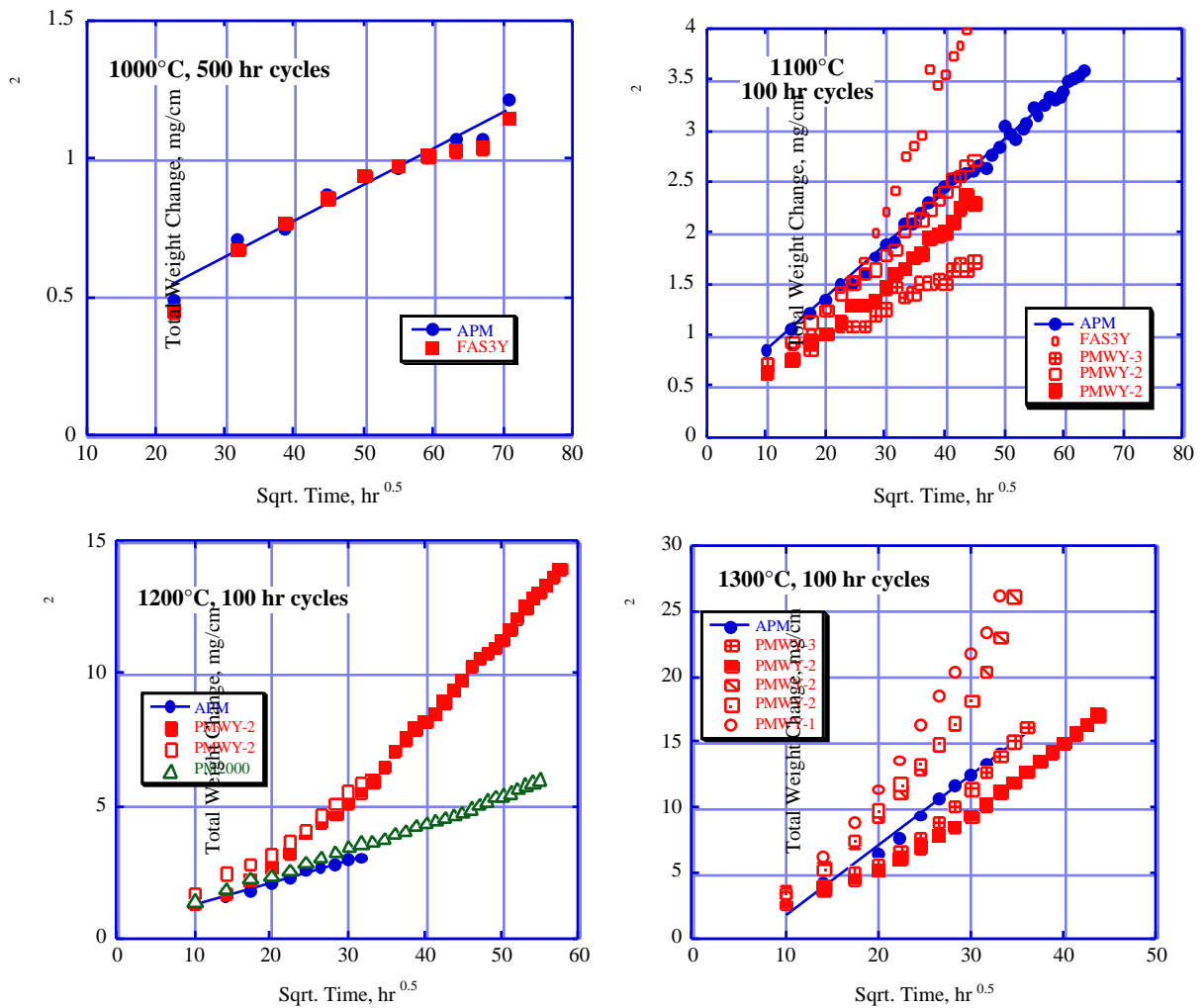


Figure 5. Summary of cyclic oxidation kinetics of ODS-Fe₃Al based on total weight gains (total oxygen consumption) at: (a) 1000°C; (b) 1100°C; (c) 1200°C; and (d) 1300°C. Data for Kanthal APM are included for comparison.

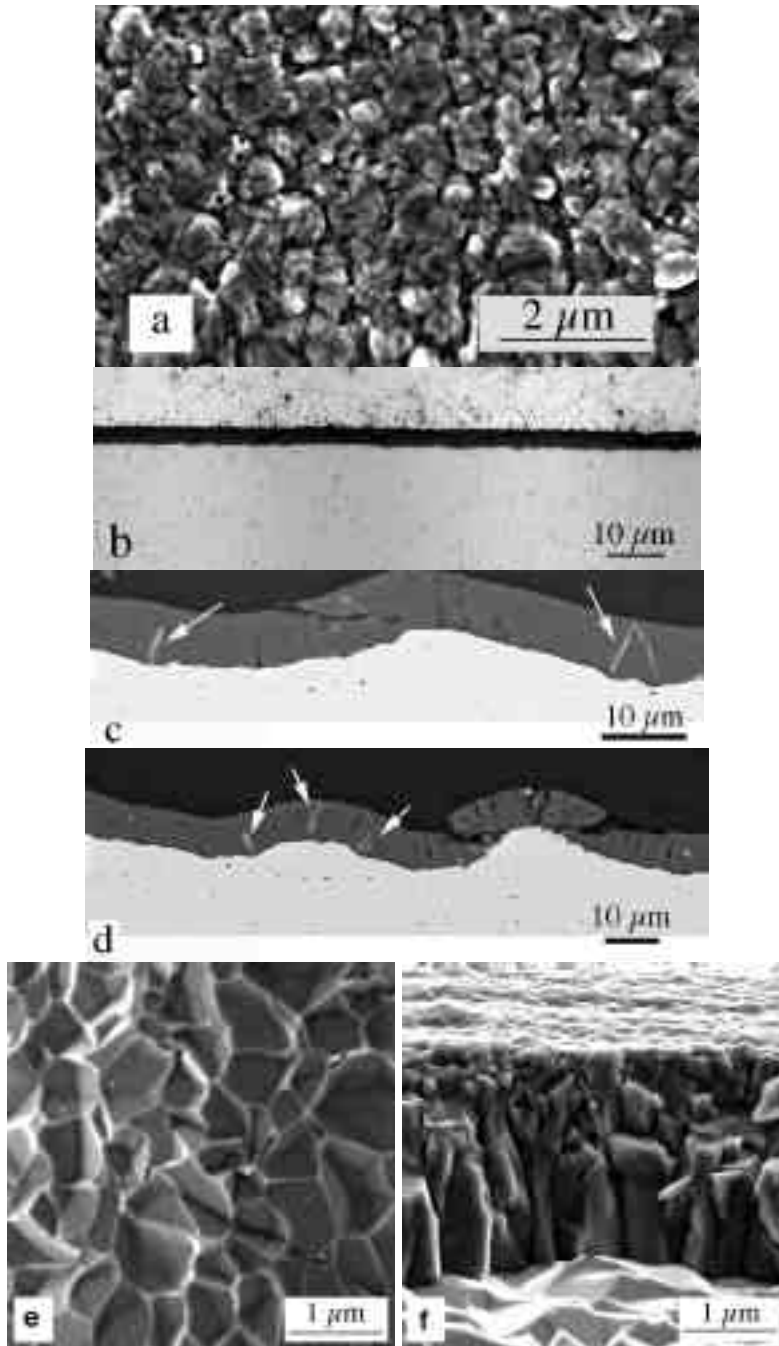


Figure 6. Scale formed on ODS-Fe₃Al alloy after isothermal exposure at 1100°C: (a) plan view, and (b)-(d) metallographic cross sections of PMWY-1 (fine-grained, not recrystallized) after 119 hr; arrows indicate Y-rich particles in the scales; (e) alloy surface beneath spalled scale, and (f) fracture section of adherent scale on PMWY-2 (recrystallized, large-grained) after 100 hr.

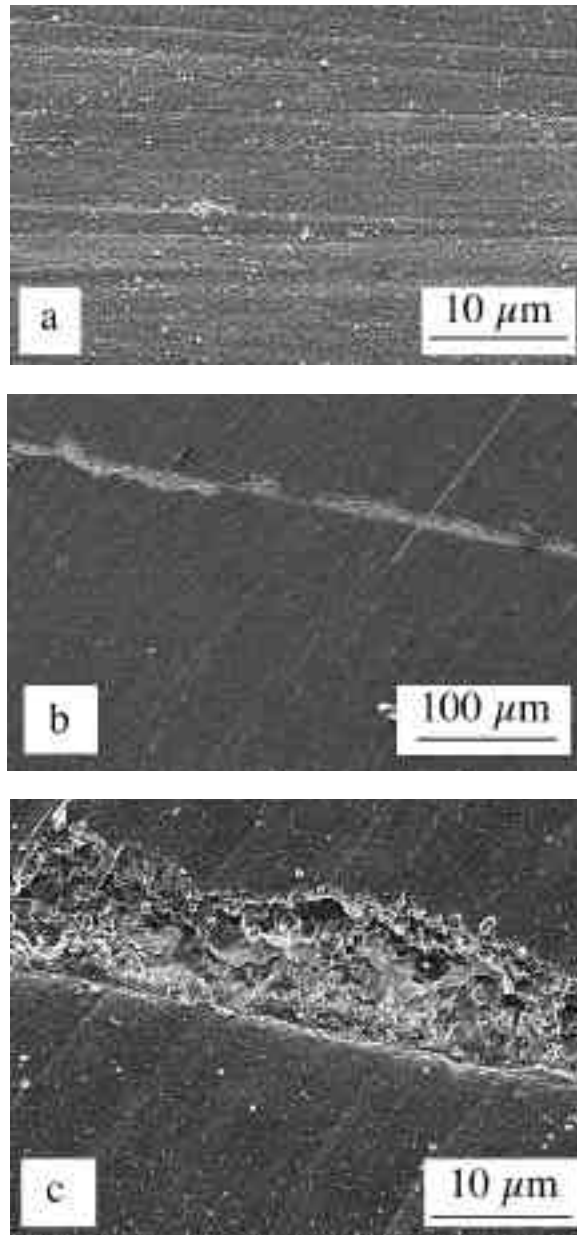


Figure 7. Plan views of scale formed on ODS-Fe₃Al alloy after isothermal exposure at 1100°C: (a) recrystallized (large-grained) PMWY-2 after 100 hr; (b) fine-grained alloy PMWY-3 after 116 hr (c) detail of (b) showing spallation trench.

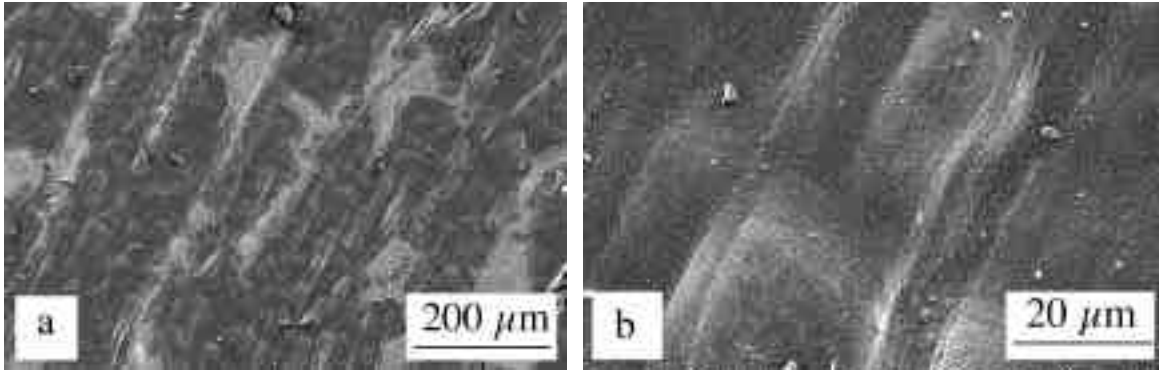


Figure 8. Topography of scale formed on fine-grained (not recrystallized) alloy PMWY-1 after 120 hr at 1200°C: (a) areas of spallation; (b) undulation in scale.

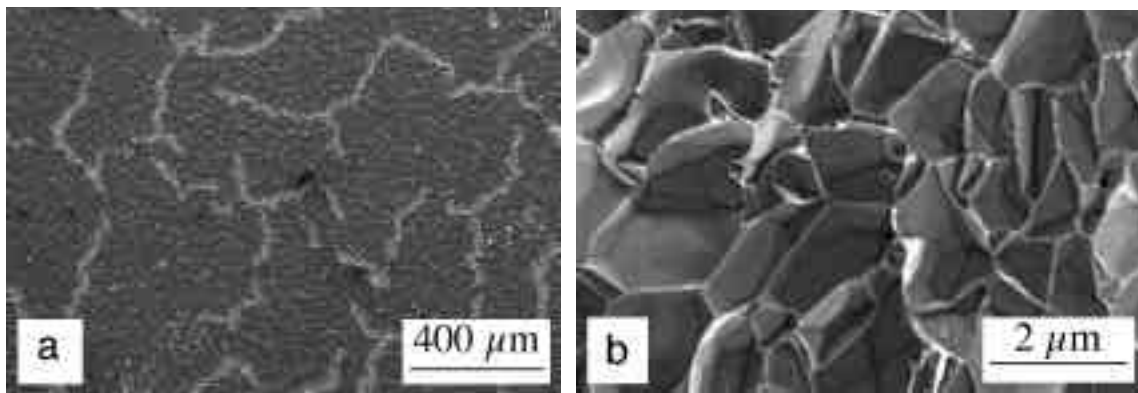
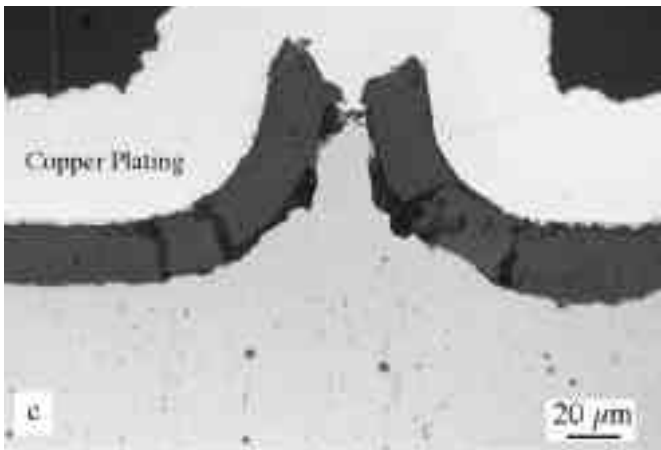
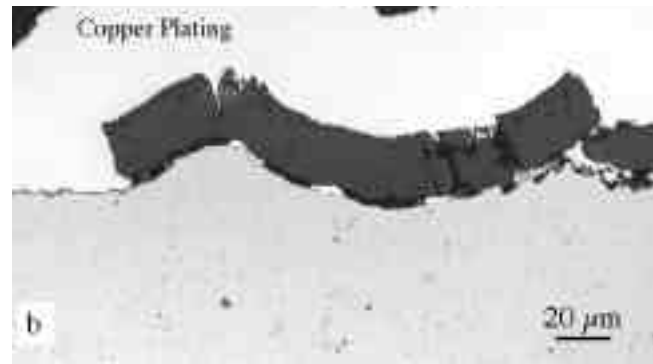
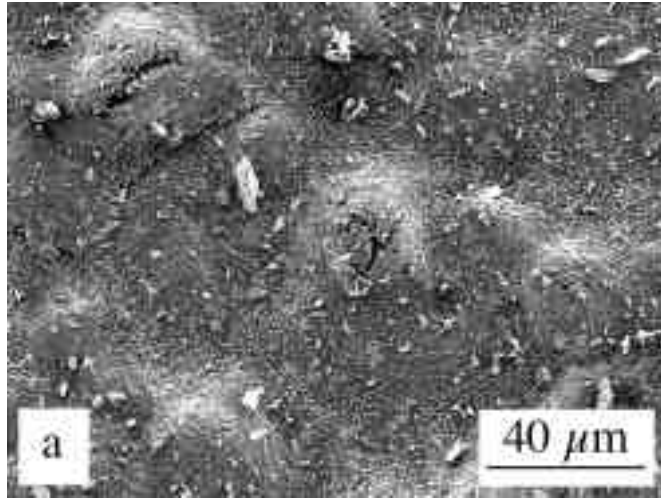


Figure 9. PMWY-2 after 100 hr of isothermal oxidation exposure at 1200°C: plan view of scale on large-grained alloy. (a) spallation; (b) alloy surface beneath spalled scale.



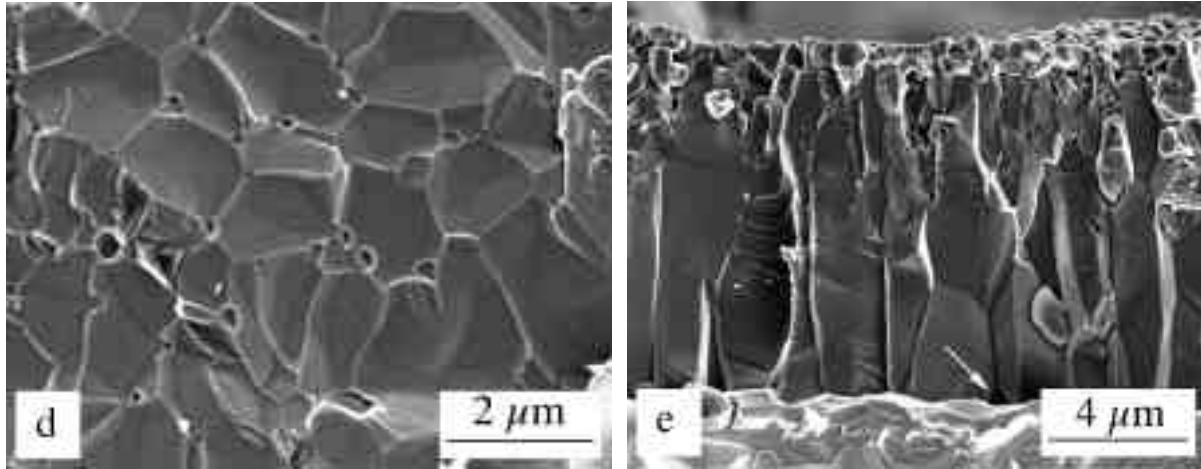


Figure 10. Scale formed on alloy PMWY-1 after 100 hr of isothermal exposure at 1300°C: (a) plan view showing undulations in the oxide and cracking; (b) metallographic cross section through an area of undulation; (c) metallographic cross section through buckled scale; (d) alloy surface beneath spalled scale; and (e) fracture section. Arrow indicates an interfacial void.

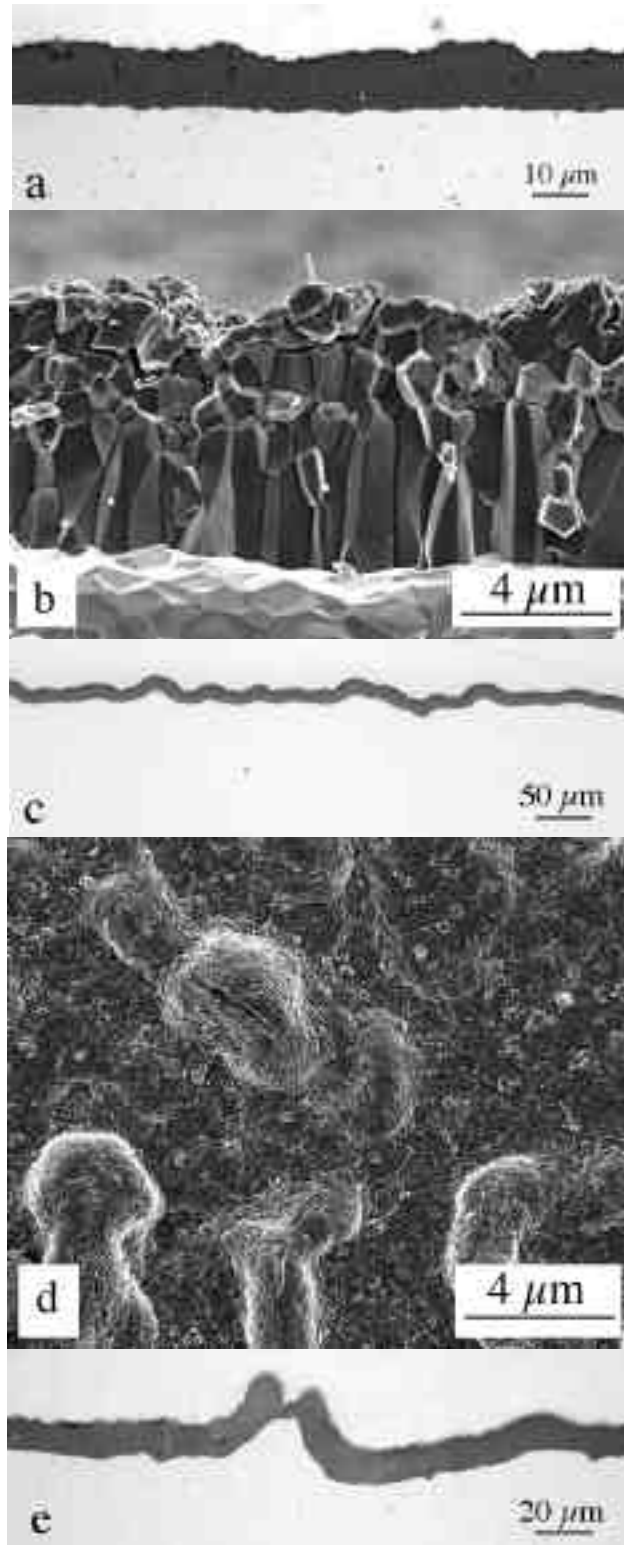


Figure 11. Scales formed on FeCrAl alloy APM after at exposure at 1200°C: (a) metallographic cross section and (b) fracture cross section after 200 h of isothermal exposure; (c) and (e) metallographic cross sections and (d) plan view after 20 x 100 h cycles at 1100°C.

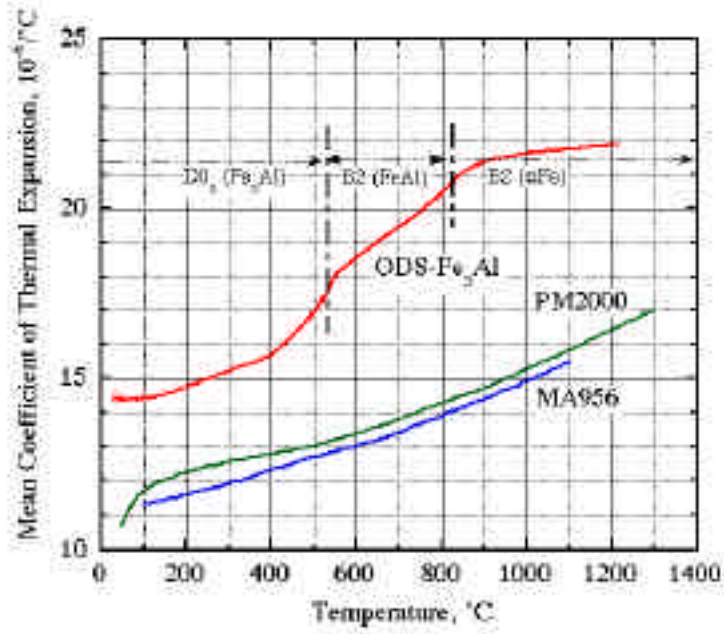


Figure 12. Comparison of mean coefficients of thermal expansion of ODS alloys with that of alumina.

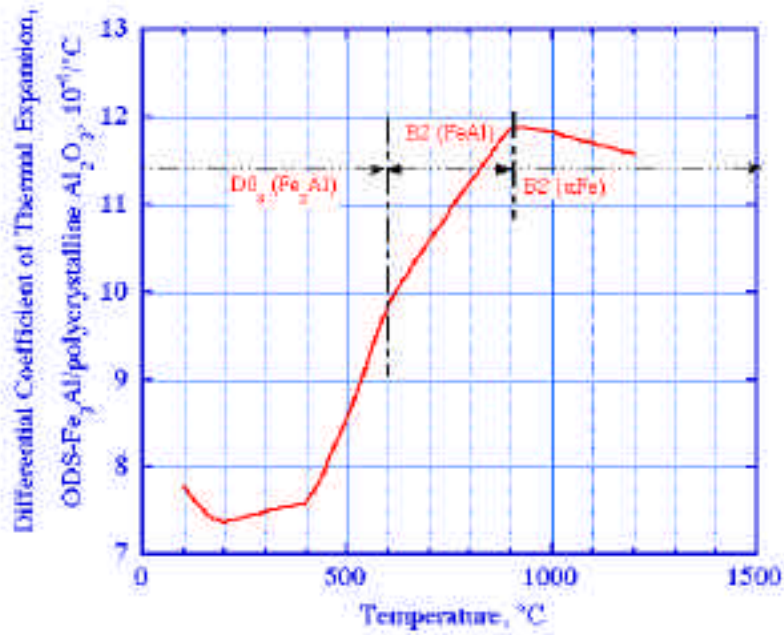


Figure 13. Variation with temperature of the difference between coefficients of thermal expansion of ODS- Fe_3Al and alumina.